Journal of Experimental and Theoretical Physics, Vol. 96, No. 4, 2003, pp. 747–756.
Translated from Zhurnal Éksperimental'noĭ i Teoreticheskoĭ Fiziki, Vol. 123, No. 4, 2003, pp. 846–856.

SOLIDS
Structure

The Structural Properties of $RbMnX_3$ (X = F, Cl, Br) Halides

V. I. Zinenko*, N. G. Zamkova, and S. N. Sofronova

Kirenskii Institute of Physics, Siberian Division, Russian Academy of Sciences, Krasnoyarsk, 660036 Russia

**e-mail: zvi@iph.krasn.ru*

Received November 27, 2002

Abstract—The results of nonempirical calculation of energies of three polytypes (cubic, two-layer hexagonal, and six-layer hexagonal) are given for $RbMnX_3$ (X = F, Cl, Br) crystals. The calculation is performed using an ionic crystal model with regard for the deformability and the dipole and quadrupole polarizabilities of ions. The behavior of these crystals under the action of hydrostatic pressure is studied. It is demonstrated that, at normal pressure, the $RbMnCl_3$ and $RbMnBr_3$ crystals have a six-layer hexagonal structure. At pressures above 11 kbar, $RbMnCl_3$ passes to a phase with a cubic structure; $RbMnBr_3$ at pressures above 90 kbar passes to a phase with a two-layer hexagonal structure. The $RbMnF_3$ crystal under normal conditions has a cubic structure and experiences no phase transformations under the effect of pressure. The obtained results are in satisfactory agreement with the known experimental data. *© 2003 MAIK "Nauka/Interperiodica".*

1. INTRODUCTION

$RbMnX_3$ (X = F, Cl, Br) crystals belong to the family of perovskite-like crystals of the general formula ABX_3. The structures of these compounds may be represented as a three-dimensional packing of rhombohedral layers of AX_3, where A is a large cation and X is an anion. Small cations B are located between layers and occupy the centers of octahedrons formed by anions. The packing of layers may be cubic (Fig. 1a) when the anion octahedrons are bound by corners, or hexagonal (*h* packing) (Figs. 1b and 1c) when the octahedrons are bound by faces. The majority of ABO_3 oxide compounds are crystallized in a perovskite structure (*c* packing); this structure and the physical properties of these substances have been fairly well studied by numerous researchers using both experimental and theoretical (including *ab initio*) methods. In compounds in which X is halogen (F, Cl, Br), both *c* packing and *h* packing may be realized, as well as mixed *ch* packings. For example, $RbMnF_3$ has a cubic perovskite structure, and $RbMnBr_3$ apparently has a hexagonal structure with a two-layer *h* packing. The $RbMnCl_3$ crystal also has a hexagonal structure, but with a six-layer packing of $RbCl_3$ layers (Fig. 1c). Here, pairs of face-bound octahedrons are interconnected via intermediate octahedrons bound to them by corners. Such a six-layer packing is designated as *hcc* packing. Almost no theoretical calculations of such hexagonal structures and of the physical properties of such compounds were performed because of the fairly complex structure and large number of atoms per unit cell.

From the standpoint of a rigid ion model, the formation of hexagonal structures is energetically disadvantageous because, in the case of the *h* packing of AX_3 layers, the ions B come very close together, which leads to a loss in the Madelung energy. Note, however, that hexagonal packings are formed, as a rule, in compounds in which X is an easily polarizable anion (Cl, Br, I). The environment of some ions in hexagonal structures is not centrally symmetric; consequently, in calculating the energy of hexagonal structures, one must take into account the polarization energy arising due to the emergence of induced electric moments (dipole, quadrupole, and so on) in such structures. The importance of inclusion of the polarization energy was emphasized in [1–4], where a number of structures (fluorite, rutile, layer structures, and the like) in compounds of the general formula MX_2 were investigated. Wilson and Madden [1] demonstrated that experimentally observed structures with a symmetry lower than cubic are stabilized only if the total crystal energy includes the contribution by the polarization energy associated with the emergence of induced dipole moments on ions of low-symmetry structures. However, all of the short-range interactions in [1] are written in a parametric form, and the number of parameters is quite large (from six to ten). Wilson *et al.* [2], who used the same parametric model of polarizable ions [3] in the investigation of different phases of ZrO_2, likewise took into account the polarization energy due to induced quadrupole moments and demonstrated that this energy played an important part in low-symmetry structures. However, Wilson *et al.* [2] themselves indicate that the

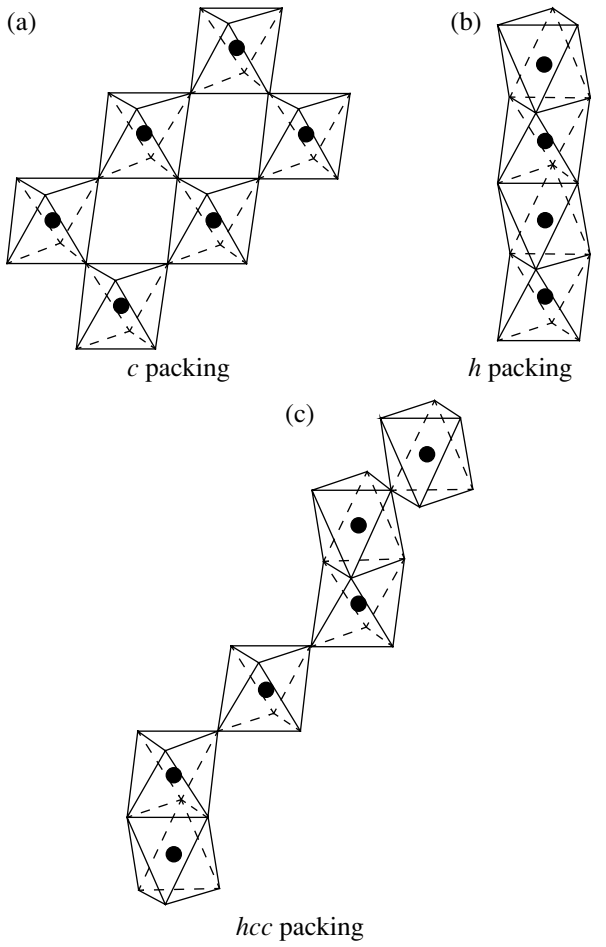

Fig. 1. The arrangement of octahedrons in different polytypes of ABX_3: (a) cubic packing (perovskite structure), (b) two-layer hexagonal packing, (c) six-layer hexagonal packing.

parametrization of the energy associated with quadrupoles is poorly validated.

The electrostatic lattice energies (Madelung energy and dipole energy) for five ideal structures with different sequences of close-packed layers of AX_3 (X = F, Cl, Br, I, O, S) and ABX_3 compounds were calculated by Weenk and Harwig [4]. They assumed the same energy of short-range spherically symmetric ion–ion interactions in different polytypes and ignored short-range dipole–dipole interactions. It was found in [4] that a two-layer hexagonal packing (*h*) turned out to be the stablest structure in ideal structural polytypes of ABX_3 compounds (including oxide compounds).

We used the nonparametric generalized Gordon–Kim model [5] to calculate the energetics of different polytypes for $RbMnX_3$ crystals, where X = F, Cl, Br. In calculating the total energy of these crystals, allowance was made for induced moments, both dipole and quadrupole. The model and method of calculation are described in Section 2. Section 3 gives the results of calculation of the total energy of three crystals, and Section 4 deals with the investigation of the effect of hydrostatic pressure. And, finally, our main results are described in Section 5.

2. MODEL: METHOD OF CALCULATION

In the Gordon–Kim model for ionic crystals, the total electron density is written as the sum of electron densities of separate ions making up a crystal,

$$\rho(\mathbf{r}) = \sum_i \rho(\mathbf{r} - \mathbf{R}_i). \tag{1}$$

The electron densities of separate ions are calculated with regard to the crystalline potential approximated by a charged Watson sphere,

$$V(r) = \begin{cases} -Z_{\text{ion}}/R_w, & r < R_w, \\ -Z_{\text{ion}}/r, & r > R_w. \end{cases} \tag{2}$$

The radii of Watson spheres in separate ions were found from the condition of minimal total energy of crystal.

In the original Gordon–Kim model, the electron density of ions was taken to be spherically symmetric; however, as was observed in [5], distortions of the electron density of any multipole symmetry are possible in an actual crystal. Ivanov and Maksimov [5] suggested a generalization of the Gordon–Kim model, enabling one to take into account multipole density distortions of any order. Here, we allowed for the dipole and quadrupole distortions of electron density,

$$\begin{aligned} \rho(\mathbf{r}) &= \sum_{l=0}^{2} \rho^{(l)}(\mathbf{r}), \\ \rho^{(l)}(\mathbf{r}) &= \sum_{m=-l}^{l} \rho^{(l)}(\mathbf{r}) Y_{lm}(\theta, \phi). \end{aligned} \tag{3}$$

Pair interactions are calculated within the theory of density functional,

$$\begin{aligned} \Phi_{ij}^{ll'} &= F\{\rho_i^{(l)}(\mathbf{r}' - \mathbf{R}_i) + \rho_j^{(l')}(\mathbf{r} - \mathbf{R}_i)\} \\ &- F\{\rho_i^{(l)}(\mathbf{r} - \mathbf{R}_i)\} - F\{\rho_j^{(l')}(\mathbf{r} - \mathbf{R}_i)\}. \end{aligned} \tag{4}$$

The total crystal energy has the form

$$E = E_0 + E_{d-d} + E_{q-q} + E_{d-q} + E_{\text{self}},$$

$$E_0 = -\frac{1}{2} \sum_{i,j=1}^{N_a} Z_i C_{ij}^{(0)} Z_j + \sum_{i,j=1}^{N_a} \Phi_{ij}^{(00)}(V_i, V_j, |\mathbf{R}_i - \mathbf{R}_j|),$$

$$E_{d-d} = \frac{1}{2}\sum_{i,j=1}^{N_a}\sum_{\alpha,\beta=1}^{3} d_i^{\alpha}\Big(\frac{\delta_{ij}}{\alpha_i^d(V_i)} + \Phi_{ij,\alpha\beta}^{(11)}(V_i, V_j, |\mathbf{R}_i - \mathbf{R}_j|) - C_{ij,\alpha\beta}^{(2)}\Big)d_j^{\beta} + \sum_{i,j=1}^{N_a}\sum_{\alpha=1}^{3} d_i^{\alpha}(\Phi_{ij,\alpha}^{(10)}(V_i, V_j, |\mathbf{R}_i - \mathbf{R}_j|) - C_{ij,\alpha}^{(1)}Z_j),$$

$$E_{q-q} = \frac{1}{2}\sum_{i,j=1}^{N_a}\sum_{\alpha,\beta,\gamma,\delta=1}^{3} q_i^{\alpha\beta}\Big[\frac{\delta_{ij}}{\alpha_i^q(V_i)} - \frac{1}{36}(\Phi_{ij,\alpha\beta\gamma\delta}^{(22)}(V_i, V_j, |\mathbf{R}_i - \mathbf{R}_j|) - C_{ij,\alpha\beta\gamma\delta}^{(4)})\Big]q_j^{(\gamma\delta)} - \frac{1}{6}\sum_{i,j=1}^{N_a}\sum_{\alpha,\beta=1}^{3} q_i^{\alpha\beta}(\Phi_{ij,\alpha\beta}^{(20)}(V_i, V_j, |\mathbf{R}_i - \mathbf{R}_j|) - C_{ij,\alpha\beta}^{(2)}Z_j), \quad (5)$$

$$E_{d-q} = -\frac{1}{6}\sum_{i,j=1}^{N_a}\sum_{\alpha,\beta,\gamma=1}^{3} q_i^{\alpha\beta} \times (\Phi_{ij,\alpha\beta\gamma}^{(21)}(V_i, V_j, |\mathbf{R}_i - \mathbf{R}_j|) - C_{ij,\alpha\beta\gamma}^{(3)})d_j^{\gamma},$$

where E_0 is the interaction energy of spherically symmetric ions; E_{d-d}, E_{q-q}, and E_{d-q} are, respectively, the energies associated with the interaction of dipole and quadrupole moments; $C_{ij}^{(n)} = \nabla^n(|\mathbf{R}_i - \mathbf{R}_j|)^{-1}$ is the long-range part of interactions; $E_{\text{self}} = \sum_{i=1}^{N_a} E_i^{\text{ion}}(V_i)$ is the ion self-energy; and N_a is the number of atoms per unit cell. In calculating the short-range interactions given by Eq. (4) for the kinetic energy, the Thomas–Fermi approximation [6] was used, and for the exchange-correlation energy, the Hedin–Lundqvist approximation [7]. The long-range interactions $C_{ij}^{(n)}$ were calculated by the Ewald method. The calculation for ion was performed using Liberman's codes [8]. The modified Sternheimer equation [9] was used to calculate the dipole α^d and quadrupole α^q polarizabilities and the respective components of electron density.

The dipole d_i^{α} and quadrupole $q_i^{\alpha\beta}$ moments were found from the condition of minimal energy with respect to the relevant moment,

$$\frac{\partial E}{\partial d_i^{\alpha}} = 0, \quad \frac{\partial E}{\partial q_i^{\alpha\beta}} = 0,$$

$$d_i^{\alpha} = \sum_{j=1}^{N_a}\sum_{\beta=1}^{3} A_{ij}^{\alpha\beta} \times \sum_{k=1}^{N_a}(\Phi_{jk,\alpha\beta}^{(10)}(V_j, V_k, |\mathbf{R}_j - \mathbf{R}_k|) - C_{jk,\beta}^{(1)}Z_k + q_i^{\alpha\beta}(\Phi_{ij,\alpha\beta\gamma}^{(21)}(V_i, V_j, |\mathbf{R}_i - \mathbf{R}_j|) - C_{ij,\alpha\beta\gamma}^{(3)})), \quad (6)$$

$$q_i^{\alpha\beta} = \frac{1}{6}\sum_{j=1}^{N_a}\sum_{\gamma\delta=1}^{3} \tilde{B}_{ij}^{\alpha\beta,\gamma\delta} \times \sum_{k=1}^{N_a}(\Phi_{jk,\gamma\delta}^{(20)}(V_j, V_k, |\mathbf{R}_j - \mathbf{R}_k|) - C_{jk,\gamma\delta}^{(1)}Z_k + \tilde{A}_{jk,\gamma\delta}),$$

$A_{ij}^{\alpha\beta}$ are elements of the matrix reciprocal to the matrix of dipole–dipole interaction in expression (5);

$$\tilde{B}_{ij}^{\alpha\beta,\gamma\delta} = \Big[\frac{\delta_{ij}}{\alpha_i^q(V_i)} - \frac{1}{36}(\Phi_{ij,\alpha\beta\gamma\delta}^{(22)}(V_i, V_j, |\mathbf{R}_i - \mathbf{R}_j|) - C_{ij,\alpha\beta\gamma\delta}^{(4)}) + \sum_{\lambda,\mu=1}^{3}(\Phi_{ij,\alpha\beta\lambda}^{(21)}(V_i, V_j, |\mathbf{R}_i - \mathbf{R}_j|) - C_{ij,\alpha\beta\lambda}^{(3)}) \times A_{ij}^{\lambda\mu}(\Phi_{ij,\mu\gamma\delta}^{(21)}(V_i, V_j, |\mathbf{R}_i - \mathbf{R}_j|) - C_{ij,\mu\gamma\delta}^{(3)})\Big]^{-1},$$

$$\tilde{A}_{jk,\gamma\delta} = \sum_{\lambda,\mu=1}^{3}(\Phi_{ij,\lambda}^{(10)}(V_i, V_j, |\mathbf{R}_i - \mathbf{R}_j|) - C_{ij,\alpha}^{(1)}Z_j) \times A_{ij}^{\lambda\mu}(\Phi_{ij,\mu\gamma\delta}^{(21)}(V_i, V_j, |\mathbf{R}_i - \mathbf{R}_j|) - C_{ij,\mu\gamma\delta}^{(3)}).$$

3. RESULTS OF CALCULATION OF TOTAL ENERGY

As was mentioned in the Introduction, ABX_3 halides may have both cubic and hexagonal structures. We will restrict ourselves to the discussion of structures of three types, namely, cubic with a perovskite structure (*c* packing) and two hexagonal with two-layer and six-layer packings (*h* and *hcc* packings, respectively), and calculate the energies for three crystals, $RbMnF_3$, $RbMnCl_3$, and $RbMnBr_3$, in these structures.

$RbMnF_3$ crystal has a structure of ideal perovskite with an O_h^1 space group and one molecule per unit

cell [10]. In this structure, the coordinates of all atoms in a unit cell are fixed,

$$\begin{array}{cccccc} \mathrm{A(Rb)} & 1(b) & 1/2 & 1/2 & 1/2 \\ \mathrm{B(Mn)} & 1(a) & 0 & 0 & 0 \\ \mathrm{X} & 3(c) & 1/2 & 0 & 0 \end{array} \qquad (7)$$

$RbMnBr_3$ crystal is characterized by a sequence of structural phase transitions, and, in the opinion of Kato *et al.* [11], the crystal structure in all phases has a distorted form of two-layer hexagonal packing. Apparently, no highly symmetric hexagonal phase with a D_{6h}^4 space group and two molecules per unit cell (Fig. 1b) is observed in this crystal up to the melting point [11]. The positions of all cations in a two-layer hexagonal packing are fixed, and the anions have one free parameter,

$$\begin{array}{cccccc} \mathrm{A(Rb)} & 2(c) & 2/3 & 1/3 & 1/4 \\ \mathrm{B(Mn)} & 2(a) & 0 & 0 & 0 \\ \mathrm{X} & 3(h) & x & 2x & 1/4 \end{array} \qquad (8)$$

In an ideal structure, $x = 1/6$.

The structure of $RbMnCl_3$ crystal is the most complex of the structures treated by us. In this crystal, a six-layer *hcc* packing with six molecules per unit cell is realized in a highly symmetric phase [12]. All ions in this structure have two crystallographically nonequivalent positions each,

$$\begin{array}{cccccc} \mathrm{A_1(Rb_1)} & 2(b) & 0 & 0 & 1/4 \\ \mathrm{A_2(Rb_2)} & 4(f) & 1/3 & 2/3 & z_1 \\ \mathrm{B_1(Mn_1)} & 2(a) & 0 & 0 & 0 \\ \mathrm{B_2(Mn_2)} & 4(f) & 1/3 & 2/3 & z_2 \\ \mathrm{X_1} & 6(h) & y_1 & 2y_1 & 1/4 \\ \mathrm{X_2} & 12(k) & y_2 & 2y_2 & z_3 \end{array} \qquad (9)$$

In this case, five free parameters are observed. In an ideal hexagonal structure, i.e., in a structure in which anions form regular octahedrons, these parameters assume the values

$$z_1 = -1/12, \quad z_2 = 1/6, \quad z_3 = 1/12,$$

$$y_1 = 1/2, \quad y_2 = 1/6.$$

We will first discuss the case of ideal structures with close-packed layers of MnX_3 (X = F, Cl, Br). In this case, the unit cell parameters *a*, *b*, and *c* for the structures being treated are related by stringent relations:

c (cubic perovskite)

$$a_c = b = c = a_0\sqrt{2};$$

h (two-layer hexagonal)

$$a_h = b = 2a_0, \quad c_h = 2a_0\sqrt{6}/3;$$

hcc (six-layer hexagonal)

$$a_h = b = 2a_0, \quad c_h = 2a_0\sqrt{6},$$

where a_0 is the distance Rb–X (X = F, Cl, Br).

Table 1. The values of the Watson sphere radii, dipole and quadrupole polarizabilities of ions, and self-energy of $RbMnX_3$ crystals

Crystal		R_w, Å	α^d, Å^3	α^q, Å^5	E_{self}, eV
$RbMnF_3$	Rb	1.98	1.12	1.97	–120521.7921
	Mn	2.88	0.78	0.85	
	F	1.32	0.79	1.01	
$RbMnCl_3$	Rb	1.75	1.14	2.02	–149971.5256
	Mn	2.22	0.84	0.96	
	Cl	1.39	3.12	7.52	
$RbMnBr_3$	Rb	1.72	1.15	2.04	–324847.5789
	Mn	2.22	0.84	7.52	
	Br	2.18	4.25	12.22	

Table 2. The calculated values (per molecule) of the total energies $E_{total} = E - E_{self}$ and of individual contributions (E^c, Madelung energy; E^s, energy of short-range spherically symmetric ion–ion interactions; E^c_{d-d}, E^c_{q-q}, and E^c_{d-q}, energies of long-range dipole–dipole, quadrupole–quadrupole, and quadrupole–dipole interactions, respectively; and E^s_{d-d}, E^s_{q-q}, and E^s_{d-q}, short-range parts of these interactions, respectively) for ideal close-packed structures

E, eV	$RbMnF_3$ a_0 = 3.11 Å			$RbMnCl_3$ a_0 = 3.63 Å			$RbMnBr_3$ a_0 = 3.85 Å		
	c	*h*	*hcc*	*c*	*h*	*hcc*	*c*	*h*	*hcc*
E^c	–40.5623	–37.6163	–39.6310	–34.6722	–32.1426	–33.8919	–32.6861	–30.3322	–32.0129
E^s	3.7548	3.8042	3.7675	2.9107	2.8909	2.8898	2.4462	2.4549	2.4604
E^c_{d-d}	0.0	–2.4809	–0.7853	0.0	–4.0991	–1.3888	0.0	–4.2000	–1.4459
E^s_{d-d}	0.0	1.8489	0.6014	0.0	2.9942	1.0591	0.0	3.0232	1.0873
E^c_{q-q}	–0.2286	–0.1249	–0.1963	–0.6357	–0.2520	–0.5269	–0.7159	–0.2804	–0.5950
E^s_{q-q}	0.2146	0.1049	0.1803	0.6341	0.2409	0.5225	0.6952	0.2747	0.5850
E^c_{d-q}	0.0	–0.0697	–0.0211	0.0	–0.1791	–0.1318	0.0	–0.2020	–0.1706
E^s_{d-q}	0.0	0.0568	0.0185	0.0	0.1547	0.1247	0.0	0.1865	0.1692
E_{total}	–36.8215	–34.4770	–36.0660	–31.7631	–30.3921	–31.3433	–30.2606	–29.0753	–29.9197

The total crystal energy given by expression (5) was minimized over the cell parameter of the cubic structure and over the radii of Watson spheres for all ions. These radii of Watson spheres were maintained for hexagonal structures as well, and, therefore, all contributions to the total crystal energy for different structures were calculated with the same values of self-energy, spherically symmetric electron density, and dipole and quadrupole polarizabilities of ions. The values of the Watson sphere radii, self-energy of ions, and dipole and quadrupole polarizabilities of ions for the crystals being treated are given in Table 1. The calculated values of individual contributions to the total energy for three structures being treated are given in Table 2.

A cubic perovskite structure (*c* packing) turns out to be more advantageous energetically for all three crystals in ideal structures with close-packed layers, although the difference between the energies of *c* packing and of two- and six-layer (*h* and *hcc*, respectively) hexagonal packing (as well as between the energies of *h* and *hcc* structures) decreases appreciably with increasing radius and polarizability of anion.

We will now discuss individual contributions to the crystal energy for different structures, as given in Table 2. One can see in this table a significant loss in the Madelung energy E^c in hexagonal *h* and *hcc* packing. At the same time, the energy of short-range interactions of the spherical part of the electron density of ions is almost the same for the structures being discussed. The main part in the stabilization of hexagonal structures is played by the polarization energy associated with the interaction between dipole distortions of the electron density of ions in noncentrally symmetric positions in hexagonal structures. Note that, if we take into account only the long-range contribution by pair interactions E^c_{d-d} to the crystal energy, a two-layer hexagonal packing turns out to be most advantageous for the $RbMnCl_3$ and $RbMnBr_3$ crystals. Energetically more advantageous for $RbMnF_3$ is a perovskite structure. The respective energies $E' = E^c + E^s + E^c_{d-d}$ (see Table 2) have the following values (in eV):

$RbMnF_3$ –36.8075(*c*), –36.2930(*h*), –36.6488(*hcc*)

$RbMnCl_3$ –31.7615(*c*), –33.3508(*h*), –32.3969(*hcc*)

$RbMnBr_3$ –30.2399(*c*), –32.0773(*h*), –30.9984(*hcc*)

Table 3. The unit cell parameters and the coordinates of ions in different structures

		$RbMnF_3$	$RbMnCl_3$	$RbMnBr_3$
		Cubic		
a_c	Calculation	4.4	5.1	5.5
	Experiment [10]	4.2		
		Two-layer hexagonal		
a_h	Calculation	5.9	6.7	6.8
	Experiment [14]			7.5
c_h	Calculation	6.0	6.9	7.2
	Experiment [14]			6.6
x/a_h	Calculation	0.1587	0.1727	0.1867
		Six-layer hexagonal		
a_h	Calculation	6.2	7.1	7.3
	Experiment [12]		7.1	
c_h	Calculation	15.7	19.0	20.8
	Experiment [12]		17.8	
y_1/a_h	Calculation	0.4880	0.5008	0.5088
	Experiment [12]		0.4928	
y_2/a_h	Calculation	0.1590	0.1456	0.1563
	Experiment [12]		0.1616	
z_1/c_h	Calculation	−0.1253	−0.1310	−0.133
	Experiment [12]		−0.0888	
z_2/c_h	Calculation	0.1510	0.1543	0.1376
	Experiment [12]		0.1603	
z_3/c_h	Calculation	0.0873	0.1000	0.106
	Experiment [12]		0.0820	

This result agrees with the findings of Weenk and Harwig [4] (in performing the calculations for fluorine compounds, they used values of a_0 and α_d different from those used by us and found almost the same energies for the *c* and *h* packings). However, one can see in Table 2 that the combined polarization energy of dipole–dipole interactions $E^c_{d-d} + E^s_{d-d}$ (note that the quantity E^s_{d-d} includes both the contributions by pair short-range interactions and the contributions by many-particle interactions, including long-range ones) is much lower than E^c_{d-d}. This is associated with the fact that the long-range field due to the lattice point charges and the field due to extended charges of an ion, which are induced on that ion when it is found in a noncentrally symmetric position, are opposite in sign and largely compensate each other. One can see in Table 2 that the contribution made to the total crystal energy by interactions associated with quadrupole distortions of the electron density of ions is small compared to the dipole–dipole energy and approximately the same for all structures being treated.

We will now turn to actual hexagonal structures. In this case, the total crystal energy given by expression (5) was minimized with respect to both the lattice parameters and all free parameters for the respective structure. In so doing, the Watson sphere radii given in Table 1 were preserved for the actual hexagonal structures as well, because our calculation results have demonstrated that, in the case of transition from one structure to another and during minimization over the lattice parameters, the Watson sphere radii either do not change at all or change insignificantly, even in the case

Table 4. The values of dipole and quadrupole moments of ions in different structures (in atomic units)

		$RbMnF_3$	$RbMnCl_3$	$RbMnBr_3$
		Cubic		
q_{zz}	X	0.0745	0.068	−0.309
		Two-layer hexagonal		
d	Rb	0.00	0.00	0.00
	Mn	0.00	0.00	0.00
	X	0.191	0.620	0.965
q_{xx}	Rb	0.025	0.004	−0.016
	Mn	−0.030	−0.032	−0.033
	X	0.044	−0.247	–1.183
q_{yy}	Rb	0.025	0.004	−0.016
	Mn	−0.031	−0.034	−0.035
	X	−0.059	−0.125	0.031
		Six-layer hexagonal		
d	Rb_1	0.0	0.0	0.0
	Rb_2	0.166	0.197	0.230
	Mn_1	0.0	0.0	0.0
	Mn_2	0.014	0.267	0.064
	X_1	0.102	0.372	0.520
	X_2	0.062	0.477	0.808
q_{xx}	Rb_1	0.029	0.065	0.077
	Rb_2	0.011	0.021	0.029
	Mn_1	0.059	0.136	0.146
	Mn_2	−0.024	−0.054	−0.056
	X_1	0.006	−0.077	−0.361
	X_2	−0.047	−0.318	0.299
q_{yy}	Rb_1	0.028	0.065	0.077
	Rb_2	0.011	0.021	0.029
	Mn_1	0.059	0.136	0.146

of a six-layer hexagonal structure with two nonequivalent positions of ions.

Table 3 gives the calculated parameters of structures along with all of the available experimental data. The predicted unit cell parameters agree with the experimental data within 1 to 8%. The greatest difference is observed in the case of determining the parameter c_h for hexagonal structures (6–8%). The calculated six-layer hexagonal structures are more extended along the z axis than the experimentally obtained structures. The agreement between the calculated coordinates of ions in a unit cell and the experimentally observed positions is within the same limits; in such a way, the ion shifts exhibit the same tendency as that observed experimentally.

The calculated values of dipole and quadrupole moments of ions for three structures are given in Table 4. Note that, in hexagonal structures, the total dipole moment of the unit cell is zero. The tensors of quadrupole moments were reduced to the principal axes, with two of three principal values being independent, $q_{zz} = -(q_{xx} + q_{yy})$. In a cubic structure, $q_{xx} = q_{yy} =$

Table 5. The calculated values (per molecule) of the total energies $E_{total} = E - E_{self}$ and individual contributions (designations are the same as in Table 2)

E, eV	$RbMnF_3$			$RbMnCl_3$			$RbMnBr_3$		
	c	*h*	*hcc*	*c*	*h*	*hcc*	*c*	*h*	*hcc*
E^c	–40.5623	–39.1902	–40.3444	–34.6722	–32.6301	–33.8317	–32.6861	–29.0245	–31.3275
E^s	3.7548	5.0400	3.9007	2.9107	3.1097	2.8239	2.4462	1.9673	2.4971
E^c_{d-d}	0.0	–2.4313	–0.2443	0.0	–4.1234	–0.8318	0.0	–4.4966	–1.3753
E^s_{d-d}	0.0	2.0824	0.1405	0.0	2.8193	0.1261	0.0	1.8115	–0.1070
E^c_{q-q}	–0.2286	–0.1247	–0.2044	–0.6357	–0.1133	–0.4500	–0.7159	–0.03979	–0.4177
E^s_{q-q}	0.2146	0.1167	0.1870	0.6341	0.0778	0.4072	0.6952	–0.2429	0.2511
E^c_{d-q}	0.0	–0.0812	–0.0095	0.0	–0.1207	–0.0850	0.0	–0.1175	–0.1515
E^s_{d-q}	0.0	0.0748	0.0073	0.0	0.1046	0.0563	0.0	0.0061	0.0591
E_{total}	–36.8215	–34.5136	–36.5671	–31.7631	–30.8761	–31.7850	–30.2606	–30.1364	–30.5716

$-q_{zz}/2$. The calculated unit cell parameters, the coordinates of ions, and the values of dipole and quadrupole moments were used to calculate individual contributions and the total energy for three crystals in two hexagonal structures; the results are given in Table 5.

One can see in Table 5 that, in the case of hexagonal structures, the crystal lattice relaxation to equilibrium values of the unit cell parameters and coordinates of ions in the lattice brings about a redistribution of the values of different contributions to the total crystal energy and brings about a still finer (compared to ideal packings) balance between these contributions. In a $RbMnF_3$ crystal, the cubic phase with a perovskite structure, in accordance with the experimental results of Copla *et al.* [10], remains more advantageous compared to nonideal hexagonal structures, although the values of the energies of the latter (compared to the energies of ideal structures) are much closer to the value of the energy of cubic structure.

In the $RbMnCl_3$ crystal, in accordance with the experimental results of Goodyear *et al.* [12], a structure with a six-layer *hcc* packing turns out to be stablest, although the energy of cubic *c* packing is very close to the energy of the latter hexagonal structure. Note that, in our calculation, the energetic advantage of a six-layer hexagonal structure compared to a cubic perovskite structure is caused by the contributions made to the total crystal energy by quadrupole–quadrupole and quadrupole–dipole interactions. The polarization energy associated with dipole distortions of the electron density of ions proves insufficient for the stabilization of the hexagonal structure in this crystal.

The dipole contribution to the total crystal energy stabilizes the six-layer hexagonal structure in $RbMnBr_3$. The energy of the *hcc* structure in this crystal is much lower than those of the *c* and *h* structures. The energetic advantage of the six-layer hexagonal structure in the $RbMnBr_3$ crystal is defined by two factors: first, the higher dipole polarizability of bromine ion results in a greater contribution by the dipole energy compared to such contribution in compounds with fluorine and chlorine; and, second, the shifts of ions in $RbMnBr_3$ are such that the difference between the Madelung energies of the *c* and *hcc* structures in this compound is much less than in $RbMnCl_3$.

Note that the results of this calculation demonstrate that, for all three crystals being treated, the two-layer hexagonal structure turns out to be energetically disadvantageous compared both to the cubic perovskite structure and to the six-layer hexagonal structure.

4. PHASE TRANSITIONS UNDER PRESSURE

Under the effect of hydrostatic pressure, many ABX_3 halogen compounds experience phase transitions between different polytypes, preferably to structures with a large fraction of cubic-packed layers [13]. Here, we give the results of calculation of enthalpy,

$$H(\Omega) = (E(\Omega) - E_{self}) + P\Omega$$

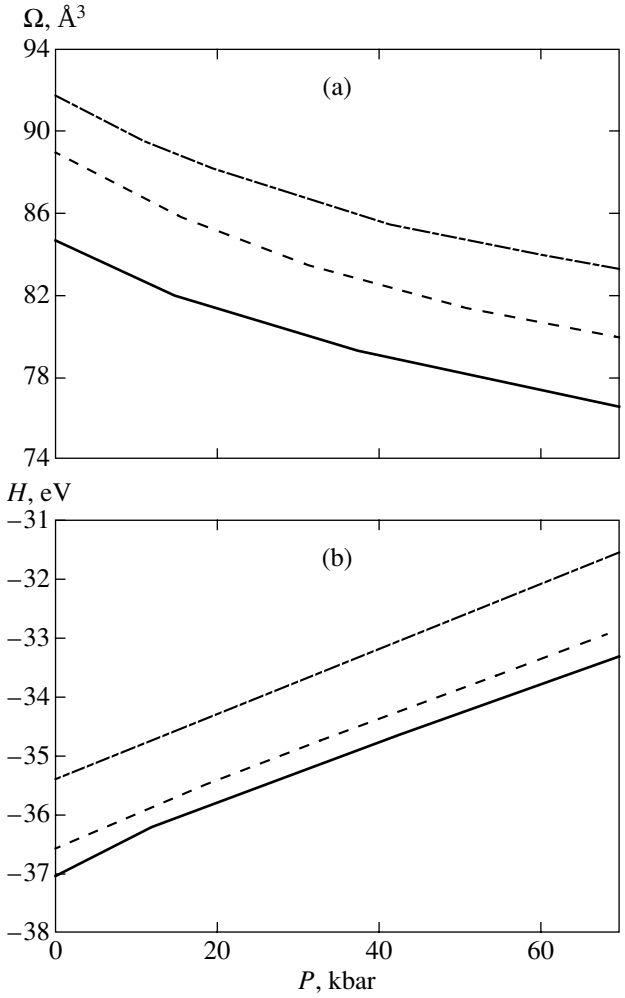

Fig. 2. (a) The equation of state and (b) the pressure dependence of enthalpy for the $RbMnF_3$ crystal. Solid curve, cubic structure; dashed curve, six-layer hexagonal structure; dot-and-dash curve, two-layer hexagonal structure.

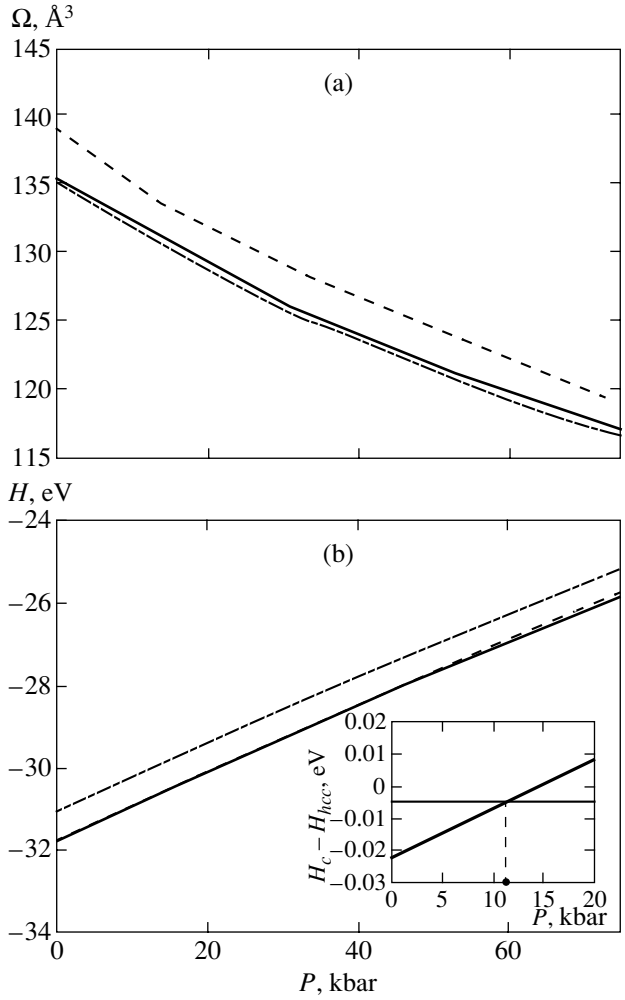

Fig. 3. (a) The equation of state and (b) the pressure dependence of enthalpy for the $RbMnCl_3$ crystal. Solid curve, cubic structure; dashed curve, six-layer hexagonal structure; dot-and-dash curve, two-layer hexagonal structure. The inset shows the pressure dependence of the difference between the enthalpies of the six-layer hexagonal and cubic structures.

($E(\Omega)$ is given by expression (5), P is the pressure, and Ω is the unit cell volume) for three crystals being treated in different structures. In deriving the equation of state, the enthalpy $H(\Omega)$ with the preassigned value of pressure P was minimized with respect to volume; in such a way, the ratio c/a between the unit cell parameters was maintained for all values of pressure. The $\Omega(P)$ equation of state and the $H(P)$ dependence of enthalpy are given in Figs. 2–4. One can see in these figures that the three crystals being treated behave differently under the effect of hydrostatic pressure. In $RbMnF_3$, the perovskite structure remains energetically advantageous under the effect of hydrostatic pressure as well. The $RbMnCl_3$ crystal at pressures above 11 kbar makes a transition from the phase with a six-layer hexagonal packing to the phase with a perovskite structure. The value of pressure $P = 11$ kbar obtained in this calculation agrees very well with the experimentally obtained value of $P = 7$ kbar [13]. The unit cell volume decreases during the $hcc \longrightarrow c$ transition, and the resultant value of the unit cell parameter of the cubic phase $a_0^{cal} = 5.094$ Å likewise agrees well with the experimentally obtained value of $a_0^{exp} = 5.058$ Å [13].

The behavior of the $RbMnCl_3$ and $RbMnBr_3$ crystals under the effect of hydrostatic pressure supports the statement made in the literature [10] about the stabilization, under pressure, of the phase with a perovskite structure in ABX_3 halides. However, in the case of the $RbMnBr_3$ crystal, the phase with a perovskite structure is not realized in this calculation up to pressures of 100 kbar (Fig. 4). Moreover, one can see in Fig. 4 that, at $P > 90$ kbar, the phase with a two-layer hexagonal packing becomes more advantageous energetically in this crystal. We are not aware of any experimental

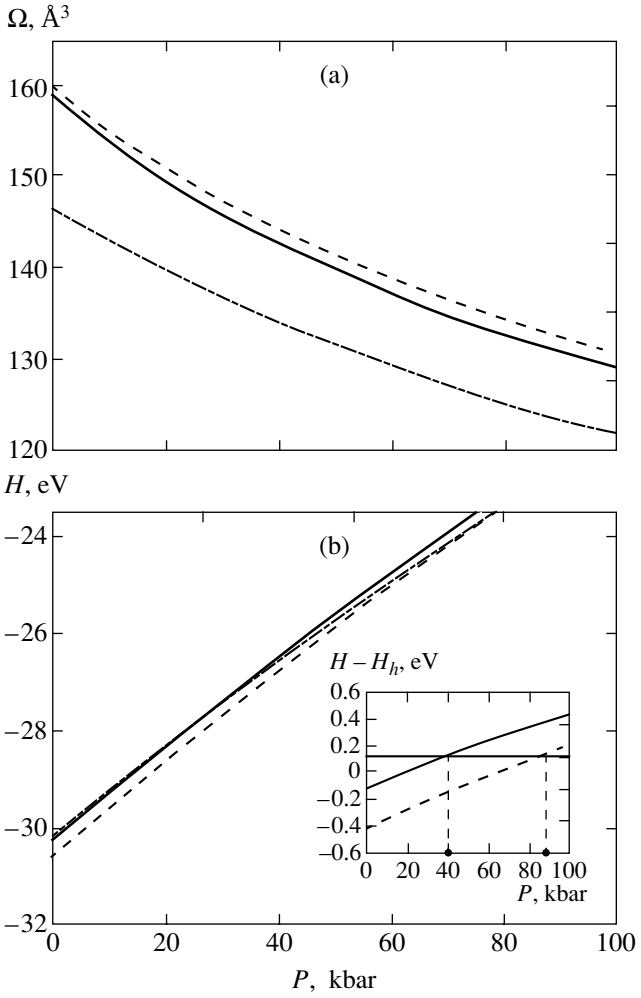

Fig. 4. (a) The equation of state and (b) the pressure dependence of enthalpy for the $RbMnBr_3$ crystal. Solid curve, cubic structure; dashed curve, six-layer hexagonal structure; dot-and-dash curve, two-layer hexagonal structure. The inset shows the pressure dependence of the difference between the enthalpies of the cubic and two-layer hexagonal structures (solid curve) and the six-layer hexagonal and two-layer hexagonal structures (dashed curve).

investigations of $RbMnBr_3$ under the effect of hydrostatic pressure.

5. CONCLUSIONS

We used a nonparametric model of ionic crystal with regard for the dipole and quadrupole polarizabilities to calculate the energies of three structures, namely, cubic (*c* packing), two-layer hexagonal (*h* packing), and six-layer hexagonal (*hcc* packing) for $RbMnF_3$, $RbMnCl_3$, and $RbMnBr_3$ crystals, and investigated the behavior of these crystals under the effect of hydrostatic pressure.

It was found that, in the $RbMnF_3$ crystal, the phase with a perovskite structure is stable both under normal conditions and under the effect of pressure; in such a way, the energy of this phase is significantly lower than the energies of the phases with *h* and *hcc* packings.

In the $RbMnCl_3$ crystal, the hexagonal *hcc* structure turns out to be stablest; under the effect of hydrostatic pressure, this crystal makes a transition to the phase with a perovskite structure. The calculated values of the phase transition pressure and of the unit cell parameter agree well with the experimental data.

In the case of the $RbMnBr_3$ crystal, we failed to observe an energetic advantage of a two-layer hexagonal structure under normal conditions. In our calculations, the energy of a six-layer hexagonal structure is always lower, in spite of the fact that the polarization energy of a two-layer hexagonal structure gives a greater negative contribution to the total crystal energy than the polarization energy in a six-layer hexagonal structure.

ACKNOWLEDGMENTS

This study was financially supported by the Russian Foundation for Basic Research–Yenisei (grant no. 02-02-97707).

REFERENCES

1. M. Wilson and P. A. Madden, J. Phys.: Condens. Matter **6**, 159 (1994).
2. M. Wilson, U. Schonberger, and M. W. Finnis, Phys. Rev. B **54**, 9147 (1996).
3. M. Wilson and P. A. Madden, J. Phys.: Condens. Matter **5**, 2687 (1993).
4. J. W. Weenk and H. A. Harwig, J. Phys. Chem. Solids **38**, 1055 (1977).
5. O. V. Ivanov and E. G. Maksimov, Zh. Éksp. Teor. Fiz. **108**, 1841 (1995) [JETP **81**, 1008 (1995)].
6. L. H. Thomas, Math. Proc. Cambr. Phil. Soc. **23**, 542 (1926); E. Fermi, Z. Phys. **48**, 73 (1928).
7. L. Hedin and B. I. Lundqvist, J. Phys. C **4**, 2064 (1971).
8. D. A. Liberman, D. T. Cromer, and J. J. Waber, Comput. Phys. Commun. **2**, 107 (1971).
9. G. D. Mahan, Phys. Rev. A **22**, 1780 (1980).
10. H. P. Copla, E. G. Sieverts, and R. H. van der Linde, Physica (Amsterdam) **51**, 573 (1971).
11. T. Kato, K. Machida, T. Ishii, and K. Iio, Phys. Rev. B **50**, 13039 (1994).
12. J. Goodyear, G. A. Steigmann, and E. M. Ali, Acta Cryst. B **33**, 256 (1977).
13. J. M. Longo and J. A. Kafalas, J. Solid State Chem. **3**, 429 (1971).
14. H. J. Seifert and E. Dan, Z. Anorg. Allg. Chem. **391**, 302 (1972).

Translated by H. Bronstein